

Article

# The Zr Modified $\gamma$ -Al<sub>2</sub>O<sub>3</sub> Catalysts for Stable Hydrolytic Decomposition of CF<sub>4</sub> at Low Temperature

Xie Zheng <sup>1,2</sup>, Kaisong Xiang <sup>2,3</sup>, Fenghua Shen <sup>1,2,\*</sup> and Hui Liu <sup>1,2,\*</sup>

<sup>1</sup> School of Metallurgy and Environment, Central South University, Changsha 410083, China; zhengxie@csu.edu.cn

<sup>2</sup> Chinese National Engineering Research Center for Control & Treatment of Heavy Metal Pollution, Changsha 410083, China; xiangkaisong@hotmail.com

<sup>3</sup> School of Chemistry and Chemical Engineering, Central South University, Changsha 410083, China

\* Correspondence: fhshen@csu.edu.cn (F.S.); leolau@csu.edu.cn (H.L.); Tel.: +86-731-88830875 (F.S. & H.L.); Fax: +86-731-88710171 (F.S. & H.L.)

**Abstract:** CF<sub>4</sub>, one of the Perfluorocompounds (PFCs), also known as a greenhouse gas with high global warming potential. In this study, Zr/ $\gamma$ -Al<sub>2</sub>O<sub>3</sub> catalysts were developed for CF<sub>4</sub> decomposition. The addition of Zr onto  $\gamma$ -Al<sub>2</sub>O<sub>3</sub> achieves a high CF<sub>4</sub> conversion efficiency of 85% at 650 °C and maintain its activity for more than 60 h, which is obviously higher than that of bare  $\gamma$ -Al<sub>2</sub>O<sub>3</sub> (50%). The mechanism involved in CF<sub>4</sub> decomposition over the Zr/ $\gamma$ -Al<sub>2</sub>O<sub>3</sub> are clarified that the surface Lewis acidity sites are the main active center for CF<sub>4</sub> directly adsorbing and decomposing. The results of NH<sub>3</sub>-TPD and FT-IR analyses suggest that the amount of Lewis acidity sites on catalyst surface increases significantly after the introduction of Zr, thereby enhancing the activity of catalyst for CF<sub>4</sub> decomposition. The results of XPS analyses confirms the electrons transfer from Zr to Al, which contribute to the increase in Lewis acidity sites. The results of this work will help the development of more effective catalysts for CF<sub>4</sub> decomposition.

**Keywords:** CF<sub>4</sub>; perfluorocompounds; catalytic decomposition; Lewis acid site; alumina; zirconia



**Citation:** Zheng, X.; Xiang, K.; Shen, F.; Liu, H. The Zr Modified  $\gamma$ -Al<sub>2</sub>O<sub>3</sub> Catalysts for Stable Hydrolytic Decomposition of CF<sub>4</sub> at Low Temperature. *Catalysts* **2022**, *12*, 313. <https://doi.org/10.3390/catal12030313>

Academic Editors: Maria Luisa Di Gioia, Luisa Margarida Martins and Isidro M. Pastor

Received: 8 February 2022

Accepted: 7 March 2022

Published: 9 March 2022

**Publisher's Note:** MDPI stays neutral with regard to jurisdictional claims in published maps and institutional affiliations.



**Copyright:** © 2022 by the authors. Licensee MDPI, Basel, Switzerland. This article is an open access article distributed under the terms and conditions of the Creative Commons Attribution (CC BY) license (<https://creativecommons.org/licenses/by/4.0/>).

## 1. Introduction

Perfluorocompounds (PFCs), such as CF<sub>4</sub>, have a high global warming potential (GWP), which is about 6500 times higher than that of CO<sub>2</sub> over a 100-year time scale. Moreover, the lifetime of PFCs can reach up to 50,000 years [1]. CF<sub>4</sub> is an extremely stable molecule because of its symmetry structure. The bond energy of C-F in CF<sub>4</sub> molecule is 543 kJ mol<sup>-1</sup>, as known as the strongest bond in organic chemistry [2,3]. The non-ferrous smelting and semiconductor industry are generally regarded as the main sources of PFCs emissions [4]. Therefore, it is of great importance to remove PFCs presented in the exhaust flue gas from non-ferrous smelting and semiconductor industry.

Several technologies have been developed for CF<sub>4</sub> emission control, such as plasma, incineration and catalytic hydrolysis [5–7]. Among them the catalytic hydrolysis has been suggested as the most economical choice to decompose CF<sub>4</sub>. Aluminum-based catalysts have displayed excellent performance in CF<sub>4</sub> decomposition due to its high specific surface area and great amount of Lewis acid [8,9]. However, Al<sub>2</sub>O<sub>3</sub> is only active for CF<sub>4</sub> decomposition at high temperature, and will fast lose its activity with the prolonging of reaction time. Recently, various methods have been developed to improve the activity of aluminum-based catalyst. El-Bahy et al. [10] researched the CF<sub>4</sub> decomposition over Ga-Al oxide catalyst. They revealed that pretreatment with sulfuric acid enhanced the Lewis acid sites, and then improved the activity and lifetime of catalyst. The above results suggest that the amount of Lewis acid sites represent the key property of catalysts for C-F activation.

Some mixed oxides exhibit strong surface acidity due to the generation of excess negative or positive charge in the model structure of the binary oxides [11]. Reddy et al. [12]

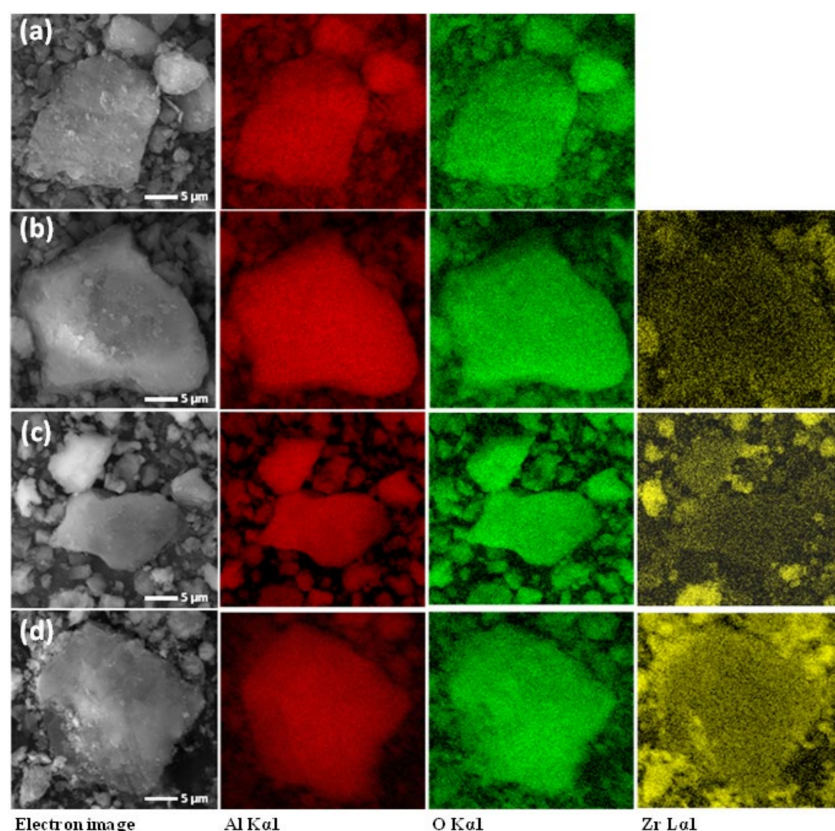
found that Zr-Al had strong acidic, since the exposed  $\text{Al}^{3+}$  and  $\text{Zr}^{4+}$  ions could act as Lewis acid sites. Luo et al. [13] reported an efficient Zr-Si oxide catalyst for the synthesis of furanic diesel precursor, and suggested that the addition of Zr species could enhance the formation of Lewis acid sites. Although there are varied Lewis acid type catalysts can be applied in  $\text{CF}_4$  decomposition, but they often require a high reaction temperature (over  $700\text{ }^\circ\text{C}$ ) to decompose the strong C-F bond. Takita et al. [14] researched the catalytic decomposition of  $\text{CF}_4$  over metal phosphate-based catalysts including phosphates of Ca, B, Fe, Zn, Bi, and Ni, and found that none of them were active at temperature lower than  $700\text{ }^\circ\text{C}$ . Xu et al. [15] studied the decomposition of  $\text{CF}_4$  over  $\gamma\text{-Al}_2\text{O}_3$  modified by several metal elements, and found that the addition of Zn and Ni could enhance the stability of catalysts, but such catalysts were only effective at high temperature ( $750\text{ }^\circ\text{C}$ ).

In view of the above reasons, a series of Zr/ $\text{Al}_2\text{O}_3$  catalysts were developed to decompose  $\text{CF}_4$  at lower temperature, i.e., under  $650\text{ }^\circ\text{C}$ . The aim of this work is to investigate the precise role of Zr/ $\text{Al}_2\text{O}_3$  in  $\text{CF}_4$  decomposition. The physicochemical properties of catalysts were characterized by different techniques. This study provided in-sights in catalytically decomposing  $\text{CF}_4$  over Zr/ $\text{Al}_2\text{O}_3$ .

## 2. Results and Discussion

### 2.1. Characterization of Catalysts as Prepared

The elemental composition and distribution of fresh catalysts is measured by SEM-EDS, as Figure 1 and Table 1. The microscopic images of bare  $\gamma\text{-Al}_2\text{O}_3$  (Figure 1a) exhibits the disorder structure consist of irregular blocky particles with rough surface. All the samples containing Zr (Figure 1b–d) present morphology similar to that of alumina. It can be intuitively understood from the EDS element mapping that the existence and uniform distribution of Al and Zr.

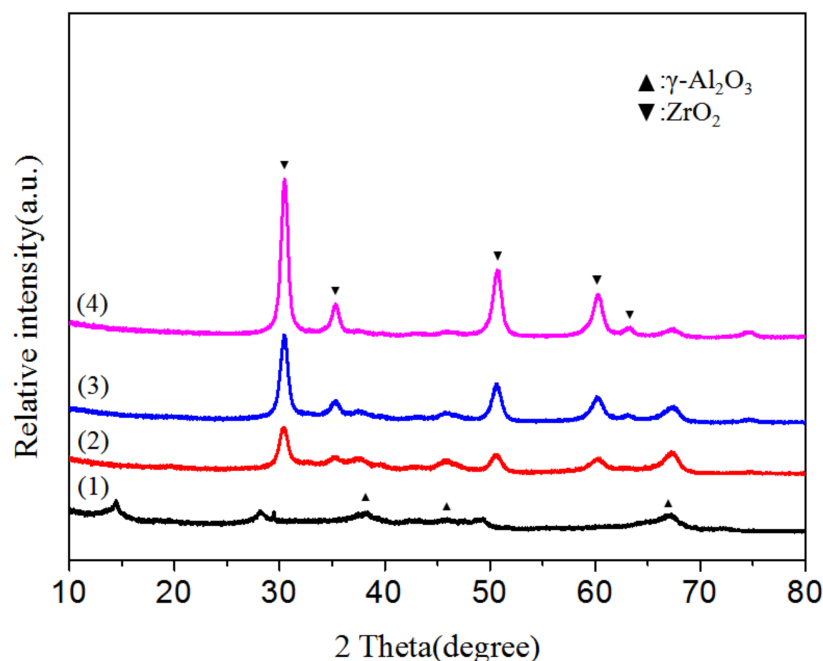


**Figure 1.** SEM-EDS mapping of (a) bare  $\gamma\text{-Al}_2\text{O}_3$ , (b) 9% Zr/ $\gamma\text{-Al}_2\text{O}_3$ , (c) 16% Zr/ $\gamma\text{-Al}_2\text{O}_3$ , (d) 35% Zr/ $\gamma\text{-Al}_2\text{O}_3$  catalysts.

**Table 1.** Elemental composition of  $\gamma$ -Al<sub>2</sub>O<sub>3</sub> and Zr/ $\gamma$ -Al<sub>2</sub>O<sub>3</sub> catalyst.

Catalyst	Al (wt.%)	O (wt.%)	Zr (wt.%)
$\gamma$ -Al <sub>2</sub> O <sub>3</sub>	26.6	74.4	/
(9%) Zr/ $\gamma$ -Al <sub>2</sub> O <sub>3</sub>	39.4	50.4	9.0
(16%) Zr/ $\gamma$ -Al <sub>2</sub> O <sub>3</sub>	30.1	53.0	16.1
(35%) Zr/ $\gamma$ -Al <sub>2</sub> O <sub>3</sub>	13.5	50.2	35.3

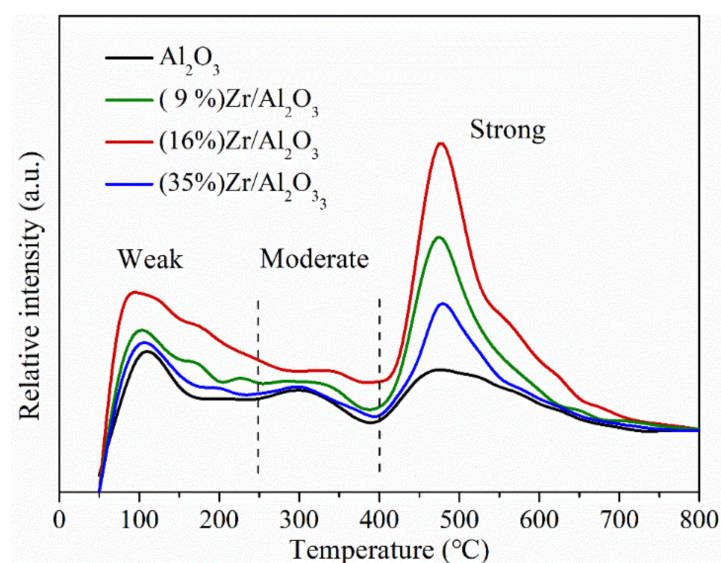
To investigate the crystal structure of the modified and bare  $\gamma$ -Al<sub>2</sub>O<sub>3</sub>, the X-ray diffraction is performed. The results are shown in Figure 2, that all catalysts contain  $\gamma$ -Al<sub>2</sub>O<sub>3</sub> (JCPDS:10-0425) [16,17]. There are four different polytypes of zirconia (i.e., monoclinic (m-ZrO<sub>2</sub>), tetragonal (t-ZrO<sub>2</sub>), cubic (c-ZrO<sub>2</sub>), and orthorhombic (o-ZrO<sub>2</sub>)) depend on the temperature and pressure [18]. As for the prepared Zr/ $\gamma$ -Al<sub>2</sub>O<sub>3</sub> catalysts, the peak of t-ZrO<sub>2</sub> (JCPDS:80-0965) is observed in XRD patterns [19], indicating the formation of zirconium oxide. The BET surface areas of the samples are listed in Table 2. The specific surface area and pore diameter of catalysts increases after the addition of Zr. The (16%) Zr/Al<sub>2</sub>O<sub>3</sub> shows the largest surface area (132 m<sup>2</sup> g<sup>-1</sup>) and pore diameter (4.1 nm). However, the surface area and pore diameter of Zr/ $\gamma$ -Al<sub>2</sub>O<sub>3</sub> decreases when further increase the amount of Zr to 35%. The BET results are consistent with previous reported, that the low content of Zr highly dispersed on the surface of aluminum oxide, the small particles on the surface provided a large surface area [20,21]. However, only a few Zr ions replaced the Al ion sites during the calcination, because the Zr ion is larger than the Al. As the content of Zr further increase, small particles will agglomerate together to form larger clusters and block the original pore, results in the surface area and pore diameter decrease. It can be anticipated that the catalyst was consist of aluminum oxide and zirconium oxide, they crystallized at the interface during the calcination [22].

**Figure 2.** XRD patterns of catalysts as prepared, (1)  $\gamma$ -Al<sub>2</sub>O<sub>3</sub>, (2) 9% Zr/ $\gamma$ -Al<sub>2</sub>O<sub>3</sub>, (3) 16% Zr/ $\gamma$ -Al<sub>2</sub>O<sub>3</sub> and (4) 35% Zr/ $\gamma$ -Al<sub>2</sub>O<sub>3</sub>.

**Table 2.** Specific surface area, pore diameter, NH<sub>3</sub>-TPD acidic sites and amount of acidic site per surface unit results for the catalyst.

Samples	BET Surface Area (m <sup>2</sup> g <sup>-1</sup> )	Pore Diameter (nm)	Amount of Acid Site (μmol g <sup>-1</sup> )/ Amount of Acid Site per Surface Unit (μmol g <sup>-1</sup> m <sup>-2</sup> )			
			Weak	Moderate	Strong	Total
			γ-Al <sub>2</sub> O <sub>3</sub>	119	3.5	235/1.97
(9%) Zr/γ-Al <sub>2</sub> O <sub>3</sub>	126	3.7	261/2.07	191/1.52	716/5.62	1168/9.27
(16%) Zr/γ-Al <sub>2</sub> O <sub>3</sub>	132	4.1	432/3.27	246/1.86	1168/8.85	1846/13.98
(35%) Zr/γ-Al <sub>2</sub> O <sub>3</sub>	89	2.8	254/2.85	206/2.31	467/5.25	927/10.42

The NH<sub>3</sub>-TPD experiments are conducted to study the acidic properties of catalysts, as shown in Table 2 and Figure 3. The desorbed ammonia is observed at 50–800 °C, according to the different thermal stability of NH<sub>3</sub> species, three kinds of acid sites are considered depending on the desorption temperature: weak acidic sites (T < 250 °C), moderate acidic sites (250 °C < T < 400 °C), and strong acidic sites (T > 400 °C) acid sites [23]. These indicate the presence of different acidic sites. The results show that the amounts of three kinds of acidic sites increased with the addition of Zr. The (16%) Zr/γ-Al<sub>2</sub>O<sub>3</sub> has the most amounts of three kinds of acidic sites especially the strong and total acidic sites, which are 2 times larger than that of bare γ-Al<sub>2</sub>O<sub>3</sub>. The (9%) Zr/γ-Al<sub>2</sub>O<sub>3</sub> has the second most amounts of weak, strong and total acidic sites. However, the increments of three kinds of acidic sites in (35%) Zr/γ-Al<sub>2</sub>O<sub>3</sub> are very slight. These finding indicates that the addition of Zr mainly increase the amount of strong and total acidic sites, but excess Zr leads to the agglomeration on surface of catalyst, which decreases the surface area and number of acidic sites. It should be noted that, the amounts of acid sites per surface unit have similar trend except the (35%) Zr/γ-Al<sub>2</sub>O<sub>3</sub>, but it can be predicted that the catalytic performance of it is limited by its small specific surface area. The above results suggest that the addition of Zr strongly enhances the surface acidity of aluminum oxide. With the addition of Zr to aluminum oxide, it generates excess negative or positive charge in the binary oxides [24]. The exposed Zr<sup>4+</sup> and Al<sup>3+</sup> can act as Lewis acids, meanwhile, they absorb electrons to generate more Lewis acid centers on the surface of catalysts. Moreover, previous research has reported that the increase of Zr in the Al<sub>2</sub>O<sub>3</sub> catalysts favored the formation of tetra- and, mainly, penta-coordinated Al species, which are considered as potential Lewis acid sites [25], therefore, increase the acidity of catalysts.

**Figure 3.** NH<sub>3</sub>-TPD profiles of catalysts.

In order to gain more information of acidic properties of catalysts, the FT-IR spectra of pyridine adsorption experiments are conducted, as shown in Figure 4. Spectra are recorded over a frequency range of 1400–1700  $\text{cm}^{-1}$ , where characteristic vibration modes of adsorbed pyridine will appear. The characteristic peaks at 1450  $\text{cm}^{-1}$ , 1491  $\text{cm}^{-1}$ , 1577  $\text{cm}^{-1}$  and 1611  $\text{cm}^{-1}$  can be assigned to the Lewis acid sites, whereas no peak of Bronsted acid sites 1545  $\text{cm}^{-1}$  is observed [15,25]. The modified  $\gamma\text{-Al}_2\text{O}_3$  exhibited more Lewis acid sites than the bare  $\gamma\text{-Al}_2\text{O}_3$ , especially (16%)  $\text{Zr}/\gamma\text{-Al}_2\text{O}_3$ , shows the most peak intensity.

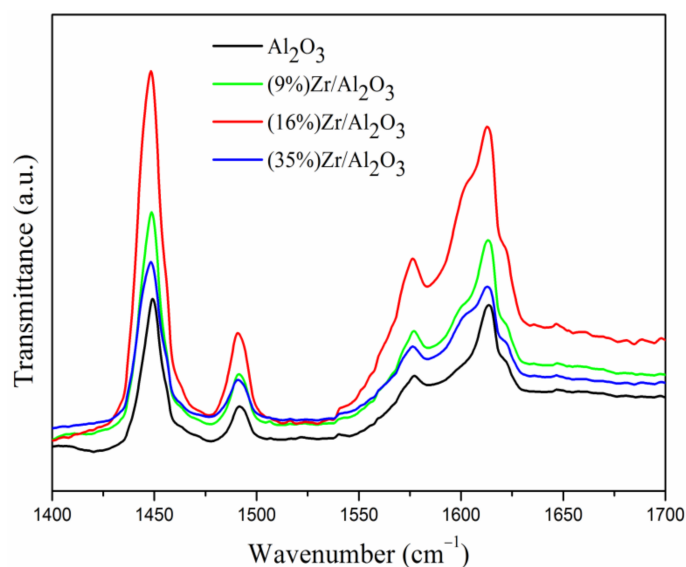


**Figure 4.** FT-IR spectra of pyridine adsorption on  $\gamma\text{-Al}_2\text{O}_3$  and  $\text{Zr}/\gamma\text{-Al}_2\text{O}_3$ .

## 2.2. Catalytic Performance of $\text{CF}_4$ Decomposition

The conversion reaction of  $\text{CF}_4$  over catalysts are conducted at 650  $^\circ\text{C}$  for 300 min, as shown in Figure 5. The initial conversion over (16%)  $\text{Zr}/\gamma\text{-Al}_2\text{O}_3$  reaches 85%, which is much higher than that over bare  $\gamma\text{-Al}_2\text{O}_3$  (50%). Furthermore, the initial conversion over (9%)  $\text{Zr}/\gamma\text{-Al}_2\text{O}_3$  and (36%)  $\text{Zr}/\gamma\text{-Al}_2\text{O}_3$  are 64% and 48%, respectively. The bare  $\text{ZrO}_2$  exhibits no catalytic activity. Therefore, (16%)  $\text{Zr}/\gamma\text{-Al}_2\text{O}_3$  is chosen as the representative sample, and then the effects of temperature on  $\text{CF}_4$  conversion over bare  $\gamma\text{-Al}_2\text{O}_3$  and (16%)  $\text{Zr}/\gamma\text{-Al}_2\text{O}_3$  are investigated, as shown in Figure 6, the (16%)  $\text{Zr}/\gamma\text{-Al}_2\text{O}_3$  catalyst exhibits much better catalytic performance.

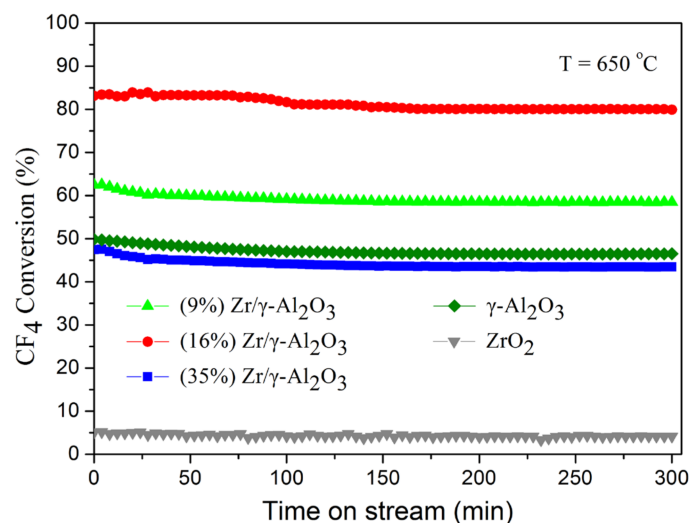


**Figure 5.**  $\text{CF}_4$  conversion reaction over different loading  $\text{Zr}/\gamma\text{-Al}_2\text{O}_3$  catalyst.

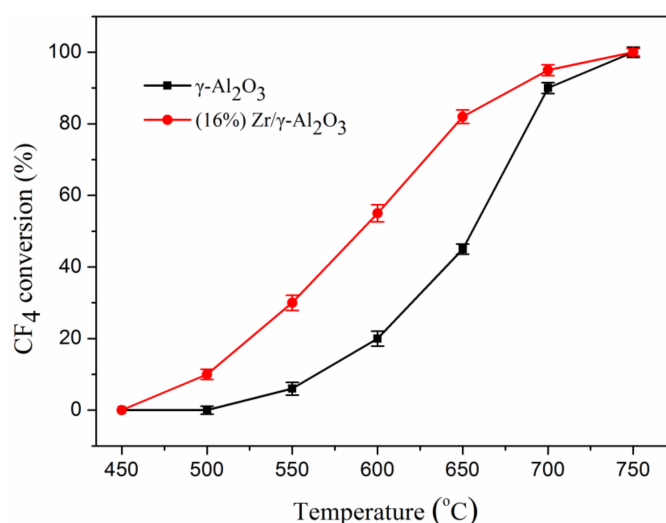


**Figure 6.** CF<sub>4</sub> conversion reaction over  $\gamma\text{-Al}_2\text{O}_3$  and Zr/ $\gamma\text{-Al}_2\text{O}_3$  catalyst.

The long-term tests are conducted to investigate the stability of catalysts, as shown in Figure 7. The (16%) Zr/ $\gamma\text{-Al}_2\text{O}_3$  catalyst exhibits excellent catalytic activity and stability compares to other works listed in Table 3. With time increasing, the catalytic efficiency of bare  $\gamma\text{-Al}_2\text{O}_3$  decreases rapidly from 30 h (42%) to 60 h (8%) while the efficiency of (16%) Zr/ $\gamma\text{-Al}_2\text{O}_3$  still remains 76%. The large difference between the conversion performances and stabilities in CF<sub>4</sub> decomposition are due to the modification by Zr element, which provides more Lewis acidic sites.

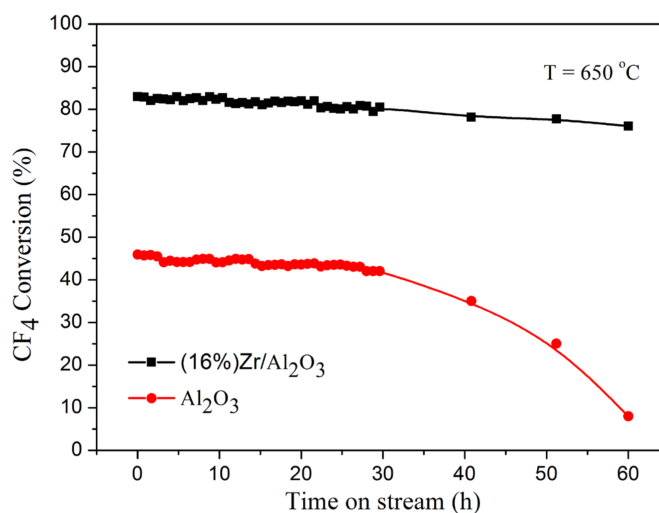


**Figure 7.** CF<sub>4</sub> conversion over  $\gamma\text{-Al}_2\text{O}_3$  and Zr/ $\gamma\text{-Al}_2\text{O}_3$  catalyst with time on stream.

**Table 3.** Comparison of catalytic decomposition of CF<sub>4</sub> with other works.

Catalysts	Temperature(°C)	Initial CF <sub>4</sub> Conversion	Stability	Ref
16%Zr/ $\text{Al}_2\text{O}_3$	650	85%	78% after 60 h	This work
$\gamma\text{-Al}_2\text{O}_3$	750	100%	65% after 20 h	[15]
2%Mg/ $\text{Al}_2\text{O}_3$	750	100%	60% after 30 h	[15]
10%Ce/ $\text{AlPO}_4$	700	73%	55% after 40 h	[7]
20%Ce/ $\text{Al}_2\text{O}_3$	650	55%	45% after 50 h	[22]
5%Cu-MCM-41	850	70%	/	[26]
5%Fe-MCM-41	800	81%	/	[27]
NaF-Si- $\text{Al}_2\text{O}_3$	850	80%	20% after 1 h	[28]
NaF-Si-MgO	850	100%	40% after 2 h	[28]

The correlation between  $\text{CF}_4$  conversion and amounts of different kind of acidic sites is shown in Figure 8. The  $\text{CF}_4$  conversion consist with the total and strong acidic sites, since the amount of strong acidic sites dominating over the others, we conclude that the strong acidic sites are the main factor that promotes the activity of the catalysts. Similarly, it has been reported that the Lewis acid sites and total acid sites played a promoting role in the decomposition of hydrofluorocarbons [29–31]. Thus, the  $\text{NH}_3$ -TPD and FT-IR results imply that the amount of acid sites on the  $\gamma\text{-Al}_2\text{O}_3$  could be increased by modified with species Zr and then improved the activity and stability of catalysts for  $\text{CF}_4$  hydrolytic decomposition.

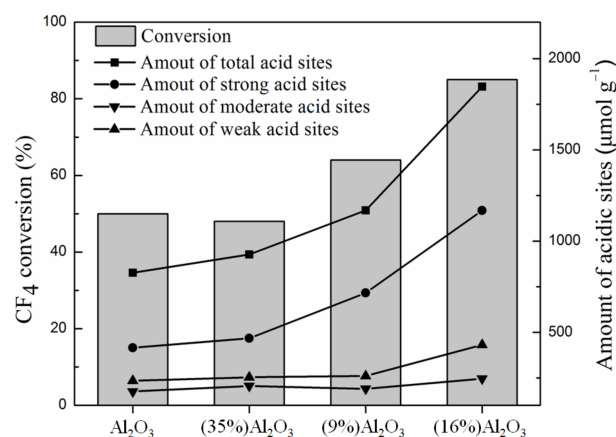


**Figure 8.** Correlation between  $\text{CF}_4$  conversion and amounts of different kind of acidic sites.

### 2.3. Mechanism Analysis of Hydrolytic Decomposition of $\text{CF}_4$

The close correlation between amount of Lewis acid sites and the conversion of  $\text{CF}_4$  strongly suggest the direct participation of the acid sites in  $\text{CF}_4$  decomposition, probably a step for subtracting fluorine atom from  $\text{CF}_4$  molecule by Lewis acid sites. To understand the mechanisms more detailly, we investigate the physicochemical properties of fresh and used catalysts. The XRD patterns of used catalysts are given in Figure 9. All the used catalysts had the characteristic peaks of  $\alpha\text{-Al}_2\text{O}_3$  and  $\text{AlF}_3$  (JCPDS:84-1672). The peak intensity of  $\alpha\text{-Al}_2\text{O}_3$  decreases with the increasing of Zr addition. Moreover, the  $\text{AlF}_3$  peak intensity of used 16% Zr/ $\gamma\text{-Al}_2\text{O}_3$  is the weakest. SEM-EDS analysis was conducted on the used catalysts as the Table 4. The results showed that the modifier Zr could inhibit the formation of  $\text{AlF}_3$  on the surface of catalysts, the amount of F on used 16% Zr/ $\text{Al}_2\text{O}_3$  catalyst is the lowest in all used catalysts, which showed a good agreement with the stability test. It can be speculated that  $\text{ZrO}_2$  on the  $\gamma\text{-Al}_2\text{O}_3$  surface prevent the formation of  $\alpha\text{-Al}_2\text{O}_3$  and  $\text{AlF}_3$  to some extent during the  $\text{CF}_4$  decomposition reaction.

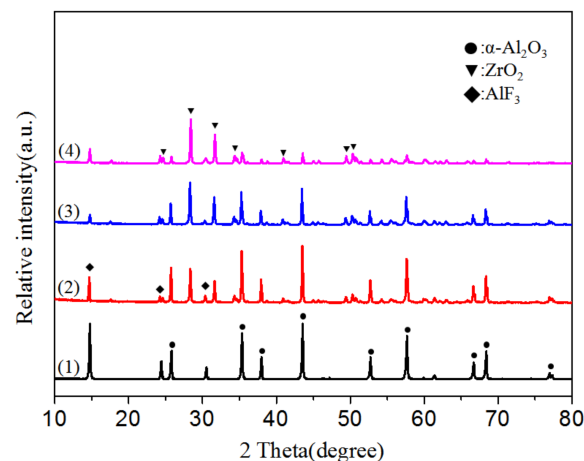


**Figure 9.** X-ray diffraction (XRD) patterns of the used catalysts, (1)  $\gamma\text{-Al}_2\text{O}_3$ , (2) 9% Zr/ $\gamma\text{-Al}_2\text{O}_3$ , (3) 16% Zr/ $\gamma\text{-Al}_2\text{O}_3$  and (4) 35% Zr/ $\gamma\text{-Al}_2\text{O}_3$ .

**Table 4.** EDS analysis of used catalysts.

Catalyst	Fluorine (Weight %)
$\gamma$ -Al <sub>2</sub> O <sub>3</sub>	27.1
(9%) Zr/ $\gamma$ -Al <sub>2</sub> O <sub>3</sub>	23.6
(16%) Zr/ $\gamma$ -Al <sub>2</sub> O <sub>3</sub>	11.2
(35%) Zr/ $\gamma$ -Al <sub>2</sub> O <sub>3</sub>	24.3

In order to acquire insights into the surface chemical composition of catalysts, X-ray photoelectron spectroscopy (XPS) analyses of catalysts are carried out and shown in Figure 10. The analysis of the Zr 3d core level spectra (Figure 10A) shows that two major binding energy values are located at range 182.9 to 183.1 eV and 185.2 to 185.5 eV, attributing to Zr 3d<sub>5/2</sub> and Zr 3d<sub>3/2</sub>, respectively. These binding energies are higher than that of the bulk ZrO<sub>2</sub> due to the higher electronegativity of Al in Zr-O-Al bond, an Al-O bond around Zr is expected to withdraw more electron density than a Zr-O bond environment, lead to more positively charges on Zr site [32]. This will increase the amount and strength of Lewis acid sites on catalysts, which shows good agreement with the results of NH<sub>3</sub>-TPD and FTIR [33,34]. As showed in Figure 10B, for the fresh catalysts, the Al 2p core level spectra exhibit peaks located at 74.3 eV, which can be ascribed to Al-O bond [35,36]. As showed in Figure 10C, for used catalysts, another set of peaks are located in the range of 75.9 to 76.4 eV, which can be attributed to Al-F bond [35–37]. Moreover, all the peak intensities of Al-O bond are remarkably decreased with the appearance of peak ascribed to Al-F bond, except 16% Zr/Al<sub>2</sub>O<sub>3</sub> [35–37]. It indicates the formation of AlF<sub>3</sub> by the reaction between Al<sub>2</sub>O<sub>3</sub> and decomposition product HF, but in the case of 16% Zr/Al<sub>2</sub>O<sub>3</sub> catalyst, species Zr alleviate the formation of AlF<sub>3</sub> from Al<sub>2</sub>O<sub>3</sub>.

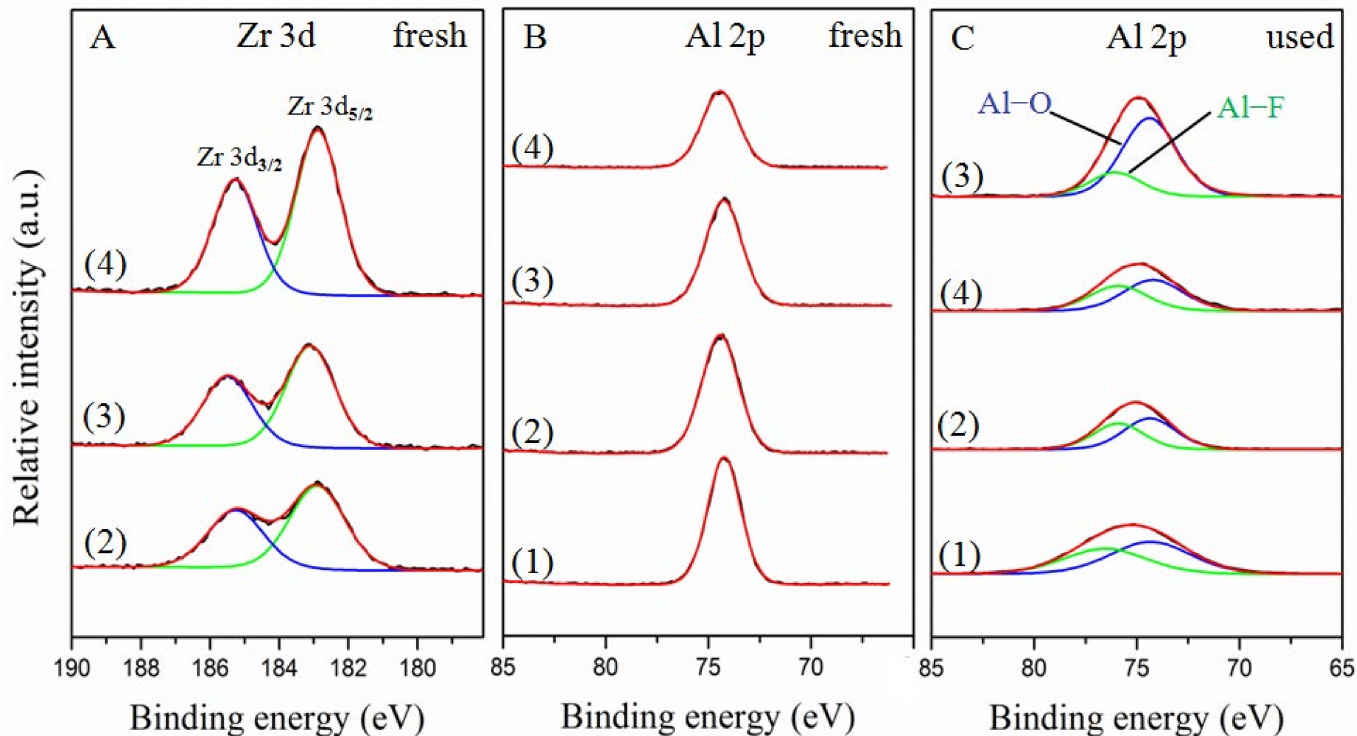


**Figure 10.** X-ray photo electron spectroscopy (XPS) spectra of catalyst, (A): Zr 3d of fresh, (B): Al 2p of fresh and (C): Al 2p of used. (1)  $\gamma$ -Al<sub>2</sub>O<sub>3</sub>, (2) 9% Zr/ $\gamma$ -Al<sub>2</sub>O<sub>3</sub>, (3) 16% Zr/ $\gamma$ -Al<sub>2</sub>O<sub>3</sub> and (4) 35% Zr/ $\gamma$ -Al<sub>2</sub>O<sub>3</sub>.

### 3. Experimental Section

#### 3.1. Catalyst Preparation

The Zr/ $\gamma$ -Al<sub>2</sub>O<sub>3</sub> catalysts were prepared by the homogeneous co-precipitation method. An aqueous solution containing the required amount of zirconium oxychloride (ZrOCl<sub>2</sub>·8H<sub>2</sub>O) and Aluminum nitrate (Al(NO<sub>3</sub>)<sub>3</sub>·9H<sub>2</sub>O) were prepared. The solutions were hydrolyzed with dilute ammonium hydroxide under stirring until the pH of the solutions reached to 9, and then subjected to hydrothermal treatment at 90 °C for 24 h. The resulting precipitate was filtered with deionized water several times and dried for 12 h at 100 °C. Finally, the catalysts were calcined at 800 °C for 4 h in N<sub>2</sub> atmosphere.

#### 3.2. Catalytic Activity Test

In the aluminum production, the CF<sub>4</sub> generated in electrolytic cell during the anode effect, the CF<sub>4</sub> content in the flue gas is about 1%. Therefore, we simulate the industrial condition to conduct experiments. The hydrolytic decomposition of CF<sub>4</sub> was carried out in a fixed-bed reactor. The temperature was maintained at 650 °C. The gas flow consists of 1% CF<sub>4</sub>, 35% H<sub>2</sub>O, and balance by Ar. The water was pre-heated at 150 °C and then constantly introduced into the reaction system by using a syringe pump. The effluent gas was washed by aqueous potassium hydroxide to remove the produced HF, and then passed through a cold trap to remove water. Finally, the gas was analyzed by an online gas chromatography (GC-9790 II) equipped with a thermal conductivity detector (TCD) detector.

#### 3.3. Catalyst Characterization

The morphology of the samples was examined by scanning electron microscope (SEM, JSM-IT300LA, JEOL, Japan) with energy dispersive X-ray (EDX) analysis. The X-ray diffraction analysis was performed on a TTR III diffractometer (XRD, Rigaku, Japan). The chemical composition and state of the elements on catalysts surface were investigated by X-ray photoelectron spectroscopy (XPS, EscaLab 250Xi, Thermo Fisher Scientific, USA). The specific surface areas were measured with the N<sub>2</sub> adsorption method on an ASAP analyzer (BET, ASAP2020, Micromeritics, USA). Ammonia temperature programmed desorption (NH<sub>3</sub>-TPD, AutoChem II 2920, Micromeritics, USA) analyses were performed using the following procedures. A 100 mg sample was pretreated at 550 °C, with helium flow of 30 mL/min for 1h, and then cooled to 50 °C. Ammonia (10% NH<sub>3</sub>/He) was introduced to the catalyst for 1 h at 50 °C. After that, the sample was flushed with helium of 50 mL/min for 1 h to remove absorbed NH<sub>3</sub>, then the temperature was programmed to increase to 900 °C at a rate of 10 °C/min. The amount of ammonia desorbed from the catalyst was detected using TCD. Fourier transform infrared spectra (FT-IR, Nicolet iS50, Thermo Fisher, USA) of pyridine absorption was conducted using the following procedures. The sample was pressed and put into an IR cell, and then it was degassed at 400 °C under vacuum for 2 h to dehydrate. Next, the cell was cooled to room temperature, and the background signal was recorded. After that, pyridine vapor was introduced to the system until reaching adsorption equilibrium. The sample was evacuated out at 150 °C for 30 min follow by cooling down to 50 °C, and then spectral acquisition was performed.

### 4. Conclusions

We modified the alumina-based catalysts with Zr to develop an efficient catalyst for CF<sub>4</sub> hydrolytic decomposition at 650 °C. The addition of Zr increase the Lewis acid sites on the surface of catalyst. The effects of modification were confirmed by using NH<sub>3</sub>-TPD and FT-IR of pyridine adsorption methods. We achieved an excellent catalytic CF<sub>4</sub> conversion (85%) over modified catalyst. Furthermore, the decomposition efficiency of modified catalyst maintains at 76% after 60 h reaction. These results indicate that the acidity properties of catalysts are strongly improved by the addition of Zr. We also investigated the physicochemical properties of fresh and used catalysts, the results suggested that addition of Zr could inhibit the formation of AlF<sub>3</sub>.

**Author Contributions:** All authors contributed to the study conception and design, X.Z. and K.X. developed and designed the methodology of this experiment. X.Z. and F.S. prepared the original draft. H.L. supervised the project and had leadership responsibility for the research. All authors have read and agreed to the published version of the manuscript.

**Funding:** This work was financially supported by National Natural Science Foundation of China (51974378), Innovative Research Group Project of the National Natural Science Foundation of China (52121004) and Special Funding for Innovative Province Construction of Hunan (2019RS3006).

**Data Availability Statement:** Data is contained within the article.

**Conflicts of Interest:** The authors declare no competing interests.

## References

1. Mühle, J.; Ganesan, A.L.; Miller, B.R.; Salameh, P.K.; Harth, C.M.; Grealley, B.R.; Rigby, M.; Porter, L.W.; Steele, L.P.; Trudinger, C.M.; et al. Perfluorocarbons in the global atmosphere: Tetrafluoromethane, hexafluoroethane, and octafluoropropane. *Atmos. Chem. Phys.* **2010**, *10*, 5145–5164. [[CrossRef](#)]
2. O'Hagan, D. Understanding organofluorine chemistry. An introduction to the C–F bond. *Chem. Soc. Rev.* **2008**, *37*, 308–319. [[CrossRef](#)] [[PubMed](#)]
3. Hannus, I. Adsorption and transformation of halogenated hydrocarbons over zeolites. *Appl. Catal. A Gen.* **1999**, *189*, 263–276. [[CrossRef](#)]
4. Pan, K.L.; Chen, Y.S.; Chang, M.B. Effective Removal of CF<sub>4</sub> by Combining Nonthermal Plasma with  $\gamma$ -Al<sub>2</sub>O<sub>3</sub>. *Plasma Chem. Plasma Process.* **2019**, *39*, 877–896. [[CrossRef](#)]
5. Chang, M.B.; Lee, H.M. Abatement of perfluorocarbons with combined plasma catalysis in atmospheric-pressure environment. *Catal. Today* **2004**, *89*, 109–115. [[CrossRef](#)]
6. Setareh, M.; Farnia, M.; Maghari, A.; Bogaerts, A. CF<sub>4</sub> decomposition in a low-pressure ICP: Influence of applied power and O<sub>2</sub> content. *J. Phys. D Appl. Phys.* **2014**, *47*, 355205. [[CrossRef](#)]
7. Takita, Y.; Ninomiya, M.; Miyake, H.; Wakamatsu, H.; Yoshinaga, Y.; Ishihara, T. Catalytic decomposition of perfluorocarbons Part II. Decomposition of CF<sub>4</sub> over AlPO<sub>4</sub>-rare earth phosphate catalysts. *Phys. Chem. Chem. Phys.* **1999**, *1*, 4501–4504. [[CrossRef](#)]
8. Xu, X.-F.; Jeon, J.Y.; Choi, M.H.; Kim, H.Y.; Choi, W.C.; Park, Y.-K. A Strategy to Protect Al<sub>2</sub>O<sub>3</sub>-based PFC Decomposition Catalyst from Deactivation. *Chem. Lett.* **2005**, *34*, 364–365. [[CrossRef](#)]
9. Jeon, J.Y.; Xu, X.-F.; Choi, M.H.; Kim, H.Y.; Park, Y.-K. Hydrolytic decomposition of PFCs over AlPO<sub>4</sub>-Al<sub>2</sub>O<sub>3</sub> catalyst. *Chem. Commun.* **2003**, *2003*, 1244–1245. [[CrossRef](#)]
10. El-Bahy, Z.M.; Ohnishi, R.; Ichikawa, M. Hydrolysis of CF<sub>4</sub> over alumina-based binary metal oxide catalysts. *Appl. Catal. B Environ.* **2003**, *40*, 81–91. [[CrossRef](#)]
11. Rosenberg, D.J.; Coloma, F.; Anderson, J.A. Modification of the Acid Properties of Silica–Zirconia Aerogels by in situ and ex situ Sulfation. *J. Catal.* **2002**, *210*, 218–228. [[CrossRef](#)]
12. Reddy, B.M.; Sreekanth, P.M.; Yamada, Y.; Kobayashi, T. Surface characterization and catalytic activity of sulfate-, molybdate- and tungstate-promoted Al<sub>2</sub>O<sub>3</sub>-ZrO<sub>2</sub> solid acid catalysts. *J. Mol. Catal. A Chem.* **2005**, *227*, 81–89. [[CrossRef](#)]
13. Luo, Y.-J.; Zhou, Y.-H.; Huang, Y.-B. A New Lewis Acidic Zr Catalyst for the Synthesis of Furanic Diesel Precursor from Biomass Derived Furfural and 2-Methylfuran. *Catal. Lett.* **2019**, *149*, 292–302. [[CrossRef](#)]
14. Takita, Y.; Morita, C.; Ninomiya, M.; Wakamatsu, H.; Nishiguchi, H.; Ishihara, T. Catalytic Decomposition of CF<sub>4</sub> over AlPO<sub>4</sub>-Based Catalysts. *Chem. Lett.* **1999**, *28*, 417–418. [[CrossRef](#)]
15. Xu, X.-F.; Jeon, J.Y.; Choi, M.H.; Kim, H.Y.; Choi, W.C.; Park, Y.-K. The modification and stability of  $\gamma$ -Al<sub>2</sub>O<sub>3</sub> based catalysts for hydrolytic decomposition of CF<sub>4</sub>. *J. Mol. Catal. A Chem.* **2007**, *266*, 131–138. [[CrossRef](#)]
16. Medeiros, R.L.; Figueredo, G.P.; Macedo, H.P.; Oliveira, Â.A.; Rabelo-Neto, R.C.; Melo, D.M.; Braga, R.M.; Melo, M.A. One-pot microwave-assisted combustion synthesis of Ni-Al<sub>2</sub>O<sub>3</sub> nanocatalysts for hydrogen production via dry reforming of methane. *Fuel* **2021**, *287*, 119511. [[CrossRef](#)]
17. Romano, P.N.; Filho, J.F.S.D.C.; de Almeida, J.M.A.R.; Sousa-Aguiar, E.F. Screening of mono and bimetallic catalysts for the dry reforming of methane. *Catal. Today* **2021**. [[CrossRef](#)]
18. Jomard, G.; Petit, T.; Pasturel, A.; Magaud, L. First-principles calculations to describe zirconia pseudopolymorphs. *MRS Online Proc. Libr.* **1997**, *492*, 79–84. [[CrossRef](#)]
19. Janampelli, S.; Darbha, S. Highly efficient Pt-MoOx/ZrO<sub>2</sub> catalyst for green diesel production. *Catal. Commun.* **2019**, *125*, 70–76. [[CrossRef](#)]
20. Li, L.; Huo, M.; Zhang, Y.; Li, J. Synthesis of nickel catalysts supported on Zr-doped ordered mesoporous Al<sub>2</sub>O<sub>3</sub> and their catalytic performance for low-temperature CO<sub>2</sub> reforming of CH<sub>4</sub>. *J. Porous Mater.* **2017**, *24*, 1613–1625. [[CrossRef](#)]
21. Patel, S.; Pant, K.K. Influence of preparation method on performance of Cu(Zn)(Zr)-alumina catalysts for the hydrogen production via steam reforming of methanol. *J. Porous Mater.* **2006**, *13*, 373–378. [[CrossRef](#)]
22. Song, J.-Y.; Chung, S.-H.; Kim, M.-S.; Seo, M.-G.; Lee, Y.-H.; Lee, K.-Y.; Kim, J.-S. The catalytic decomposition of CF<sub>4</sub> over Ce/Al<sub>2</sub>O<sub>3</sub> modified by a cerium sulfate precursor. *J. Mol. Catal. A Chem.* **2013**, *370*, 50–55. [[CrossRef](#)]

23. Ma, L.; Cheng, Y.; Cavataio, G.; McCabe, R.W.; Fu, L.; Li, J. In situ DRIFTS and temperature-programmed technology study on  $\text{NH}_3$ -SCR of  $\text{NO}_x$  over Cu-SSZ-13 and Cu-SAPO-34 catalysts. *Appl. Catal. B Environ.* **2014**, *156–157*, 428–437. [[CrossRef](#)]
24. Xia, Y.; Hua, W.; Gao, Z. A new catalyst for n-butane isomerization: Persulfate-modified  $\text{Al}_2\text{O}_3$ - $\text{ZrO}_2$ . *Appl. Catal. A Gen.* **1999**, *185*, 293–300. [[CrossRef](#)]
25. Garcia-Sancho, C.; Jimenez-Gomez, C.P.; Viar-Antunano, N.; Cecilia, J.A.; Moreno-Tost, R.; Merida-Robles, J.M.; Requires, J.; Maireles-Torres, P. Evaluation of the  $\text{ZrO}_2/\text{Al}_2\text{O}_3$  system as catalysts in the catalytic transfer hydrogenation of furfural to obtain furfuryl alcohol. *Appl. Catal. A Gen.* **2021**, *609*, 117905. [[CrossRef](#)]
26. Jing-Long, H.; Shiue, A.; Yu-Yun, S.; Den-Wei, H.; Chang-Tang, C. Catalytic decomposition of  $\text{CF}_4$  over copper promoted mesoporous catalysts. *Sustain. Environ. Res.* **2013**, *23*, 307–314.
27. Chen, C.-K.; Shiue, A.; Huang, D.-W.; Chang, C.-T. Catalytic Decomposition of  $\text{CF}_4$  Over Iron Promoted Mesoporous Catalysts. *J. Nanosci. Nanotechnol.* **2014**, *14*, 3202–3208. [[CrossRef](#)]
28. Xu, X.; Niu, X.; Fan, J.; Wang, Y.; Feng, M.  $\text{CF}_4$  decomposition without water over a solid ternary mixture consisting of NaF, silicon and one metal oxide. *J. Nat. Gas Chem.* **2011**, *20*, 543–546. [[CrossRef](#)]
29. Takita, Y.; Tanabe, T.; Ito, M.; Ogura, M.; Muraya, T.; Yasuda, S.; Nishiguchi, H.; Ishihara, T. Decomposition of  $\text{CH}_2\text{FCF}_3$  (134a) over Metal Phosphate Catalysts. *Ind. Eng. Chem. Res.* **2002**, *41*, 2585–2590. [[CrossRef](#)]
30. Swamidoss, C.M.A.; Sheraz, M.; Anus, A.; Jeong, S.; Park, Y.-K.; Kim, Y.-M.; Kim, S. Effect of  $\text{Mg}/\text{Al}_2\text{O}_3$  and Calcination Temperature on the Catalytic Decomposition of HFC-134a. *Catalysts* **2019**, *9*, 270. [[CrossRef](#)]
31. Takita, Y.; Moriyama, J.-I.; Nishiguchi, H.; Ishihara, T.; Hayano, F.; Nakajo, T. Decomposition of  $\text{CCl}_2\text{F}_2$  over metal sulfate catalysts. *Catal. Today* **2004**, *88*, 103–109. [[CrossRef](#)]
32. Armelao, L.; Eisenmenger-Sittner, C.; Groenewolt, M.; Gross, S.; Sada, C.; Schubert, U.; Tondello, E.; Zattin, A. Zirconium and hafnium oxoclusters as molecular building blocks for highly dispersed  $\text{ZrO}_2$  or  $\text{HfO}_2$  nanoparticles in silica thin films. *J. Mater. Chem.* **2005**, *15*, 1838–1848. [[CrossRef](#)]
33. García-Sancho, C.; Moreno-Tost, R.; Mérida-Robles, J.; Santamaría-González, J.; Jiménez-López, A.; Maireles-Torres, P. Zirconium doped mesoporous silica catalysts for dehydration of glycerol to high added-value products. *Appl. Catal. A Gen.* **2012**, *433–434*, 179–187. [[CrossRef](#)]
34. Salas, P.; Wang, J.; Armendariz, H.; Angeles-Chavez, C.; Chen, L. Effect of the Si/Zr molar ratio on the synthesis of Zr-based mesoporous molecular sieves. *Mater. Chem. Phys.* **2009**, *114*, 139–144. [[CrossRef](#)]
35. Limcharoen, A.; Pakpum, C.; Limsuwan, P. An X-ray Photoelectron Spectroscopy Investigation of Redeposition from Fluorine-based Plasma Etch on Magnetic Recording Slider Head Substrate. *Proc. Eng.* **2012**, *32*, 1043–1049. [[CrossRef](#)]
36. Kim, S.W.; Park, B.J.; Kang, S.K.; Kong, B.H.; Cho, H.K.; Yeom, G.Y.; Heo, S.; Hwang, H. Characteristics of  $\text{Al}_2\text{O}_3$  gate dielectrics partially fluorinated by a low energy fluorine beam. *Appl. Phys. Lett.* **2008**, *93*, 191506. [[CrossRef](#)]
37. Zhang, T.; Park, J.Y.; Huang, W.; Somorjai, G.A. Influence of reaction with  $\text{XeF}_2$  on surface adhesion of Al and  $\text{Al}_2\text{O}_3$  surfaces. *Appl. Phys. Lett.* **2008**, *93*, 141905. [[CrossRef](#)]